Coastal Engineering in Japan, Vol. 36, No. 1, 1993

WAVE-INDUCED OSCILLATIONS IN HARBOURS WITH DISSIPATING QUAYS

Chung-Ren Chou[1]
Wen-Yu Han[2]

ABSTRACT

A method based on a boundary element method was described for predicting wave height distributions in a harbour of arbitrary shape and variable water depth. Effects of partial reflection along harbour and breakwater boundaries were considered by involving an energy dissipation coefficient in boundary conditions. Numerical results on wave heights within a rectangular harbour were presented for cases of fully absorbing, fully reflecting and partially reflecting boundaries. A realistic harbour geometry was selected for trial computations, and results of the computations were verified through hydraulic model experiments.

Keywords: harbour oscillation, boundary element method, energy dissipating coefficient

I. INTRODUCTION

One of the major objectives in harbour engineering is the maintenance of a relatively undisturbed water surface within regions of interest. The most effective way to achieve this is to reserve some area in a harbour for natural dissipation. However, almost all the harbours, especially the fishery harbours, in Taiwan have insufficient space to allow for wave energy dissipation. An alternative way is to dispose the vertical dissipating quays in harbours, as many examples are found both in Taiwan and in Japan. However, the choice of the most suitable location and length of the dissipating structure in a harbour is rather problematic. To solve this problem, engineers have usually relied on model experiments in the past, but numerical methods have also been developed. With increasing speed of performance and lowering cost for acquisition of modern computers, numerical analyses seem to provide a potentially more economical alternative than model experiments.

Many investigators have studied various aspects of the harbour oscillation problem. Miles and Munk (1961) used a point source method to analyze harbour oscillations associated with radiation effects that expand from harbour entrance to offshore. They found the phenomenon of harbour paradox. Ippen and Goda (1963) used Fourier transformation to analyze a rectangular basin with impermeable vertical wall. Hwang and Tuck (1970) used a boundary integral method which involves the distribution of wave sources along the harbour boundary to calculate oscillations in harbours

[1]Professor, Dept. of Harbor and River Eng., National Taiwan Ocean Univ., Bee-Ning Rd. 2, Keelung 204, Taiwan.
[2]Graduate Student, ditto.

of constant depth and arbitrary shape. Lee (1971) applied Weber's solution to solve Helmholtz equation and analyzed harbour oscillation of arbitrary shape with constant water depth. Chou and Lin (1986) used a boundary element method to analyze wave-induced oscillations in a harbour of arbitrary shape with rigid quays in variable water depth.

The above studies, however, suffer some deficiencies; in other words, they are applicable either to complete reflection or to zero reflection at the harbour boundaries. In fact, reflecting boundaries are not always fully reflecting. In order to treat this problem, Berkhoff (1976) used mild-slope equation involving a partial reflection condition, that is, $\partial\phi/\partial n + \alpha k\phi = 0$ (where n is the local coordinate taken normal to a boundary and α is the complex transmission coefficient and k is the wave number), to solve wave diffraction and refraction problem in harbours with arbitrary reflective properties. Isaacson and Qu (1990) assumed that the partial reflection has no influence upon the form of a reflected wave, and related the transmission coefficient $\alpha(=\alpha_1+i\alpha_2)$ to the reflection coefficient Kr, the phase shift β associated with the reflection, and the angle γ that the incident wave train makes with the wall. Unfortunately, the phase angle β and the incident wave direction γ are difficult to determine. For special cases of β=0 and γ=0, they indicated that $\alpha_1 = 0$ and $\alpha_2 = (1 - Kr)/(1 + Kr)$.

Chou and Lin (1989) also applied a boundary element method to analyze oscillations in a harbour of arbitrary shape with constant water depth. The boundary condition at an arbitrary reflecting boundary involves an energy dissipating coefficient $\alpha(=\sqrt{1-Kr^2})$ based on the theory of energy conservation. In their study, the phase lag between incident and reflective waves was considered in the process of computing potential functions, where effects of material of dissipating structures were not included.

In this paper, an extended model for variable water depth will be presented. For verification, model experiments were carried out and compared with numerical predictions.

II. THEORETICAL ANALYSIS

Figure 1 schematically shows a harbour configuration under consideration. A Cartesian coordinate system is employed, the origin of which is located at o with the z-axis vertically upwards. As shown in the figure, the flow field is divided into two regions by a pseudo-boundary surface Γ_1: Region I is an open sea region with constant depth, and Region II is a harbour basin bounded by Γ_1 and the harbour and breakwater boundaries, with variable water depth. The presence of a harbour and breakwaters affects waves in both the regions. However, if the pseudo-boundary Γ_1 is sufficiently far away from the structures (by $0.5L$ or more, where L is incident wave length), wave scattering due to them can be neglected in Region I.

Usual assumptions of the fluid being inviscid and incompressible and the flow being irrotational are adopted here. We consider linear waves, having angular frequency $\sigma(=2\pi/T,\ T$ is the wave period) and amplitude ζ_o, incident from the open sea at an angle of ω against the x-axis. Fluid motions in both the regions will then have velocity potentials, $\Phi(x, y, z; t)$, in the following form:

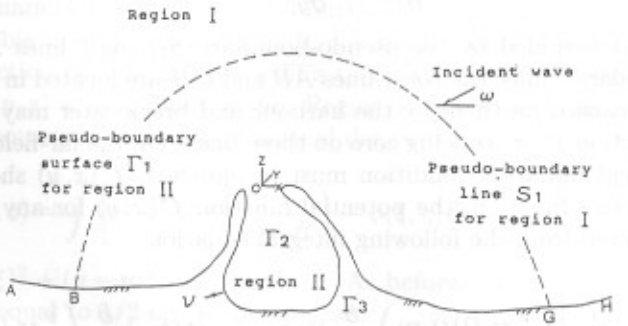

Fig. 1 Definition sketch.

$$\Phi(x,y,z;t) = \frac{g\zeta_0}{\sigma}\phi(x,y,z)\exp(-i\sigma t) \tag{1}$$

where g is the gravitational acceleration, and $\phi(x,y,z)$ must satisfy the Laplace equation

$$\frac{\partial^2\phi}{\partial x^2} + \frac{\partial^2\phi}{\partial y^2} + \frac{\partial^2\phi}{\partial z^2} = 0 \tag{2}$$

2.1 Potential function in Region I

Since wave scattering due to depth variation is neglected in this region, the resultant potential function for Region I, $\phi_o(x,y,z)$, can be expressed as

$$\phi_o(x,y,z) = \{f^o(x,y) + f^*(x,y)\}\frac{\cosh k(z+h)}{\cosh kh} \tag{3}$$

where h is the water depth, k is the wave number ($\sigma^2 h/g = kh\tanh kh$), $f^o(x,y)$ is the potential function of the incident waves, and $f^*(x,y)$ is the potential function representing combined reflection and diffraction of waves caused by the harbour, breakwater and bottom topography.

For sinusoidal incident waves, the corresponding water surface elevations can be expressed as

$$\zeta_i(x,y;t) = \zeta_0\cos[k(x\cos\omega + y\sin\omega) + \sigma t], \qquad (0 \le \omega \le \pi) \tag{4}$$

The potential function of the incident wave $f^o(x,y)$ is then given by

$$f^o(x,y) = -i\cdot\exp[-ik(x\cos\omega + y\sin\omega)] \tag{5}$$

Substituting Eq. (3) into Eq. (2), we obtain the potential function for $f^*(x,y)$, which satisfies the Helmholtz equation of the following form:

$$\frac{\partial^2 f^*}{\partial x^2} + \frac{\partial^2 f^*}{\partial y^2} + k^2 f^* = 0 \tag{6}$$

Region I is bounded by the pseudo-boundary S_1, coast lines $\overline{AB}$ and $\overline{GH}$, and far-field boundary. Since the coast lines $\overline{AB}$ and $\overline{GH}$ are located in the open sea area, disturbances caused on them by the harbour and breakwater may be negligible, the potential function $f^*(x,y)$ being zero on these lines. On the far-field boundary, where the Sommerfeld radiation condition must be satisfied, $f^*(x,y)$ should also be zero. Applying Green's function, the potential function $f^*(x,y)$ for any point in Region I can be calculated from the following integral equation:

$$cf^*(x,y) = \int_{s_1} \left[\left(\frac{i}{4} H_0^{(1)}(kR) \right) \frac{\partial}{\partial \nu} f^*(\xi,\eta) - f^*(\xi,\eta) \frac{\partial}{\partial \nu} \left(\frac{i}{4} H_0^{(1)}(kR) \right) \right] ds \tag{7}$$

where $f^*(\xi,\eta)$ is the potential function specified by the geometric condition of the boundaries in Region I, $\partial f^*(\xi,\eta)/\partial \nu$ $(= \overline{f}^*)$ is its normal derivative with ν the local normal coordinate to the boundary taken outwards, $H_0^{(1)}$ is the zeroth order Hankel function of the first kind, and $R = [(x-\xi)^2 + (y-\eta)^2]^{1/2}$ is the distance between a point under consideration and the boundary. The factor c equals to unity within the boundary, but will have a value of $1/2$ on boundaries.

In the numerical analysis, the boundary S_1, where c = $1/2$, is discretized into M segments, each having a constant element. Equation (7) is then rewritten in a matrix form as

$$\{F^*\} = [K^*]\{\overline{F}^*\} \tag{8}$$

where

$$\begin{aligned}
&[K^*] = [H^*]^{-1}[G^*] \\
&\{F^*\} = f_j^* \\
&\{\overline{F}^*\} = \left\{ \frac{\partial F^*}{\partial \nu} \right\} = \overline{f}_j^* \qquad (j = 1, M) \\
&[H^*] = H_{ij}^* \\
&H_{ij}^* = \begin{cases} \overline{H}_{ij} & (i \neq j) \\ \overline{H}_{ij} + \frac{1}{2} & (i = j) \end{cases} \qquad (i, j = 1, M) \\
&\{G^*\} = G_{ij}^* \\
&\overline{H}_{ij} = \int_{\Gamma_j} \frac{\partial}{\partial \nu} \left(\frac{i}{4} H_0^{(1)}(kR) \right) ds \\
&G_{ij}^* = \int_{\Gamma_j} \frac{i}{4} H_0^{(1)}(kR) ds
\end{aligned}$$

in which $\{F^*\}$ and $\{\overline{F}^*\}$ are the potential function and its normal derivative on the pseudo-boundary S_1, and $[K^*]$ is a coefficient matrix related to the geometric location of S_1.

2.2 Potential function in Region II

Region II with arbitrary water depth is a closed three-dimensional domain bounded by the pseudo-boundary Γ_1, the free water surface Γ_2, the quays or breakwaters Γ_3 and an impermeable uneven sea bed Γ_4. It is stressed that Γ_3 is assumed to have an arbitrary reflection coefficient. According to Green's second identity law, velocity potential $\phi(x, y, z)$ at any point within Region II can be determined by velocity potential on the boundary and its first normal derivative as

$$c\phi(x,y,z) = \int \left[\frac{\partial \phi(\xi,\eta,\zeta)}{\partial \nu} \left(\frac{1}{4\pi R} \right) - \phi(\xi,\eta,\zeta) \frac{\partial}{\partial \nu} \left(\frac{1}{4\pi R} \right) \right] dA \tag{9}$$

where $R = [(x-\xi)^2 + (y-\eta)^2 + (z-\zeta)^2]^{1/2}$. As before, c is unity for points inside the region and is equal to $1/2$ on the boundaries.

To proceed with numerical calculation, surfaces of the boundaries Γ_1 through Γ_4, are divided into N_1 to N_4 discrete segments with constant elements. The length of each segment on Γ_2 is usually taken as $L/16$, or less, and that on Γ_4 is taken as $L/8$, or less, where L is the incident wave length. For the case that $c = 1/2$, Eq. (9) is readily expressed as

$$\{\phi\} = [K]\{\overline{\phi}\} \tag{10}$$

where

$$\begin{aligned}
&[K] = [H]^{-1}[G] \\
&\{\phi\} = \phi_j \\
&\{\overline{\phi}\} = \left\{ \frac{\partial \phi}{\partial \nu} \right\} = \overline{\phi}_j \quad (j = 1, N_1 + N_2 + N_3 + N_4) \\
&[H] = H_{ij} \qquad\qquad (i, j = 1, N_1 + N_2 + N_3 + N_4) \\
&H_{ij} = \begin{cases} \overline{H}_{ij} & (i \neq j) \\ \overline{H}_{ij} + \frac{1}{2} & (i = j) \end{cases} \\
&\{G\} = G_{ij} \\
&\overline{H}_{ij} = \int_{\Gamma_j} \frac{\partial}{\partial \nu} \left(\frac{1}{4\pi R} \right) ds \\
&G_{ij} = \int_{\Gamma_j} \frac{1}{4\pi R} ds
\end{aligned}$$

in which $\{\phi\}$ and $\{\overline{\phi}\}$ are the potential function and its normal derivative on the boundaries Γ_1 through Γ_4, and [K] is a coefficient matrix related to the geometry of the boundaries.

2.3 Boundary conditions

The boundary conditions required for the case under consideration are summarized as follows:

(1) Free surface condition

Under uniform air pressure, the boundary condition on the free water surface is given as

$$\overline{\phi} = \frac{\sigma^2}{g} \cdot \phi \qquad (z = 0) \tag{11}$$

(2) Boundary condition on the impermeable sea bed

The flow is zero in the normal direction to an impermeable sea bed, that is,

$$\overline{\phi} = 0 \tag{12}$$

(3) Boundary condition on the pseudo-boundary

Requirement of mass and energy flux continuity between Region I and Region II at the pseudo-boundary Γ_1 leads to the following expression:

$$\overline{\phi}_0(\xi, \eta, z) = \overline{\phi}(\xi, \eta, z) \tag{13}$$

$$\phi_0(\xi, \eta, z) = \phi(\xi, \eta, z) \tag{14}$$

Substituting Eq. (3) into Eq. (13), multiplying both sides by $\cosh k(z+h)$ and integrating from $-h$ to 0 with respect to z, we obtain the following relation:

$$\int_{-h}^{0} \overline{\phi}(\xi, \eta, z) \cosh k(z+h) dz = \int_{-h}^{0} [\overline{f}^o(\xi, \eta) + \overline{f}^*(\xi, \eta)] \frac{\cosh^2 k(z+h)}{\cosh kh} dz$$

By dividing the surface of the pseudo-boundary Γ_1 into N segments vertically and M segments horizontally, the above equation can be rewritten in a discretized form as

$$\overline{f}^*(\xi_i, \eta_i) = \frac{k}{N_0 \sinh kh} \sum_{j=1}^{N} \overline{\phi}(\xi_i, \eta_i, \zeta_i) \cosh k(z_j + h) \Delta z_j - \overline{f}^o(\xi_i, \eta_i)$$
$$(i = 1, 2, \cdots, M) \tag{15}$$

where $N_0 = (1/2)(1 + 2kh/\sinh 2kh)$.

Substituting Eq. (3) into Eq. (14), we obtain

$$\phi(\xi_i, \eta_i, z) = [f^o(\xi_i, \eta_i) + f^*(\xi_i, \eta_i)] \frac{\cosh k(z+h)}{\cosh kh}$$
$$(i = 1, 2, \cdots, M \times N) \tag{16}$$

and further substitution of Eqs. (8) and (15) yields the following matrix expression:

$$\{\phi_1\} = [R]\{F^o - K^* \overline{F}^o\} + C[R][K^*][Q]\{\overline{\phi}_1\} \tag{17}$$

where $C = k/(N_0 \sinh kh)$, the subscript 1 denotes functions on the boundary Γ_1, and [R] and [Q] are coefficient matrices given by

$$[R] = \begin{bmatrix} \dfrac{\cosh k(z_{11}+h)}{\cosh kh} & & 0 \\ \vdots & & \\ \dfrac{\cosh k(z_{1n}+h)}{\cosh kh} & & \\ & \ddots & \\ 0 & & \dfrac{\cosh k(z_{m1}+h)}{\cosh kh} \\ & & \vdots \\ & & \dfrac{\cosh k(z_{mn}+h)}{\cosh kh} \end{bmatrix} \tag{18}$$

$$[Q] = \begin{bmatrix} \cosh k(z_{11}+h)\Delta z_1 & \cdots & \cosh k(z_{1n}+h)\Delta z_n \\ & \ddots & \\ \cosh k(z_{m1}+h)\Delta z_1 & \cdots & \cosh k(z_{mn}+h)\Delta z_n \end{bmatrix} \tag{19}$$

Equation (17) expresses the relation between the potential function $\phi(x, y, z)$ and its derivative on the pseudo-boundary Γ_1.

(4) Boundary condition on a quay or breakwater

Assume the quay or breakwater boundary Γ_3 is impermeable and have an arbitrary reflection coefficient K_r. Since waves are reflected only partially, these structures can be treated as having conceptually an energy dissipation coefficient α, which was defined by Chou and Lin (1989) as

$$\alpha = \sqrt{1 - {K_r}^2} \tag{20}$$

The boundary condition on Γ_3 is now conveniently expressed as

$$\overline{\phi}(\xi, \eta, \zeta) = ik\alpha\phi\ (\xi, \eta, \zeta) \tag{21}$$

2.4 Equation system

To facilitate substitution of the boundary conditions, we first rewrite the governing equation, Eq. (10), into the following form:

$$[\phi_i] = [K_{ij}][\overline{\phi}_i] \quad (i, j = 1, 4) \tag{22}$$

and the unknown functions on the boundaries Γ_1 through Γ_3 are obtained from

$$[\phi_i] = [K_{ij}][\overline{\phi}_i] \quad (i, j = 1, 3) \tag{23}$$

Substitution of Eqs. (11), (17) and (21) into Eq. (23) and a little algebra lead to

$$\begin{bmatrix} [K_{11} - CRK^*Q] & \frac{\sigma^2}{g}K_{12} & ik\alpha K_{13} \\ K_{21} & \frac{\sigma^2}{g}K_{22} - I & ik\alpha K_{23} \\ K_{31} & \frac{\sigma^2}{g}K_{32} & ik\alpha K_{33} - I \end{bmatrix} \begin{bmatrix} \overline{\phi}_1 \\ \phi_2 \\ \phi_3 \end{bmatrix} = \begin{bmatrix} R[F^o - K^*\overline{F}^o] \\ 0 \\ 0 \end{bmatrix} \tag{24}$$

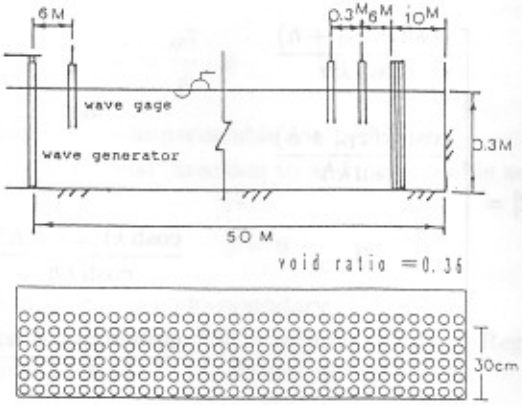

Fig. 2 Setup of two-dimensional wave flume and dissipating quay.

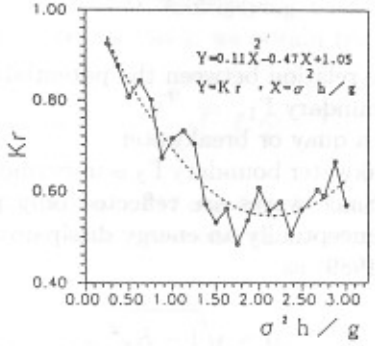

Fig. 3 Reflection coefficient of dissipating quay.

By solving the above equation, the derivative of potential functions on the boundary Γ_1 and the potential functions on boundaries Γ_2 and Γ_3 are obtained. The wave height ratio, K_d, defined as the ratio of the wave height in Region II to the incident wave height, can be calculated from

$$K_d = |\phi_2| \tag{25}$$

III. REFLECTION COEFFICIENT OF DISSIPATING STRUCTURES

To proceed with the numerical analysis, the energy dissipation coefficient α in Eq. (21) must be determined. In other words, the reflection coefficient K_r in Eq. (20) must be found empirically. This was done through experiments in a two-dimensional wave flume as schematically shown in Fig. 2. The wave flume has dimensions of 50 m in length, 1.8 m in width and 1.5 m in depth. A programmable wave generator of

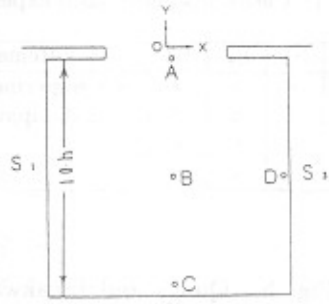

Fig. 4 Definition sketch for square harbour.

piston type is installed at one end of the flume. A dissipating model structure with a void ratio of 0.36 was located 40m away from the wave generator. The incident wave heights in the experiments ranged from 4 to 6 cm. The method of Goda and Suzuki (1976) was employed to obtain the reflection coefficients as shown in Fig. 3, where the abscissa is scaled with $\sigma^2 h/g$ and the ordinate with K_r. The dotted curve shows the best fit of the experimental data for the least square. Reflection coefficients for different frequencies determined from this empirical function will be used in the subsequent computations.

IV. NUMERICAL COMPUTATIONS

4.1 Square basin with constant water depth

As stated before, the main objective of this paper is to introduce the energy dissipation coefficient in the boundary condition. Computations were first carried out for a square basin with a width of $10h$ (h is the water depth of the open sea) and an opening width $b = 5h$ at the center of the basin, as shown in Fig. 4. The same dissipating quays as those in the two-dimensional wave flume experiment were assumed and uniform water depths in both the Regions I and II. Wave scattering due to bathymetric condition was thus eliminated.

In the numerical analysis, the boundary surfaces were divided into 1056 discrete areas with constant element (N_1=104, N_2=720, N_3=52, N_4=180, and M=2). Relationships between wave heights and frequencies at the 4 locations A, B, C and D indicated in Fig.4 were calculated for incident waves propagating perpendicularly toward the harbour entrance. The coordinates of these locations are A($0.25h$, $-0.25h$), B($0.25h$, $-5.25h$), C($0.25h$, $-9.75h$) and D($4.75h$, $-5.25h$). Distributions of wave heights were also calculated for dimensionless frequencies $\sigma^2 h/g$=1.206, 0.537 and 0.302 (wave period T=1.0, 1.5 and 2.0 sec). Table 1 shows the conditions of these computations.

4.2 A Real Harbour

Computations were also performed for an example of the Patosu fishery harbour built 3 years ago in the northern part of Taiwan. The layout and topography of

Table 1 Cases of square basin experiments.

	S1	S2	S3	Remarks
case I	×	×	×	× : impermeable quay
case II	○	○	○	○ : dissipating quay
case III	×	○	×	
case IV	○	×	○	

the harbour are given in Fig. 5. Quays and breakwaters of this fishery harbour are dissipating structures (PERFORCELL), whose reflection coefficient is estimated approximately at 0.75, the energy dissipation coefficient α being 0.661. In the numerical computation, water depth larger than 40 m was regarded as constant, and the boundary surfaces were divided into 1988 discrete segments with constant elements (N_1=152, N_2=1329, N_3=176, N_4=331, and M=2). Distributions of wave heights were calculated for incident waves propagating from 23.5° north-northeast ($\omega = 66.5^o$) toward the harbour entrance with dimensionless frequencies of $\sigma^2 h/g$ =2.518, 1.611 and 1.169 (T=0.8, 1.0 and 1.2 sec).

V. LABORATORY EXPERIMENTS

5.1 Square basin with constant water depth

Experiments were carried out in a three-dimensional wave basin, 30 m long, 25 m wide and 1 m deep, as shown in Fig. 7. The programmable wave generator is capable of generating regular and irregular waves. Water depth was kept at 0.3 m throughout the experiments. The incident wave heights ranged from 4 to 6 cm. Water surface displacements were measured with 6 capacitance-type wave gauges aligned at 20 cm spans.

In the experiments of case II in Table 1, the nondimensional frequencies of incident waves, $\sigma^2 h/g$, were varied in the range between 0.25 and 3.0 (T=2.2 to 0.63 sec), and surface elevations at the 4 locations A, B, C and D were measured for 2 to 3 times.

In the subsequent experiments, waves with $\sigma^2 h/g$ =1.206, 0.537 and 0.302 were used. Wave heights were measured at various locations in the harbour, and contour maps for wave height distributions were drawn in terms of the wave height ratio K_d, that is, the ratio of measured wave height to incident wave height.

5.2 Patosu fishery harbour

Another series of experiments were conducted using a physical model of the Patosu fishery harbour with a scale of 1/100. The water depth was 0.4 m in region I. The direction and period of incident waves were exactly the same as those in the numerical computations; the wave heights were in the range from 4 to 6 cm.

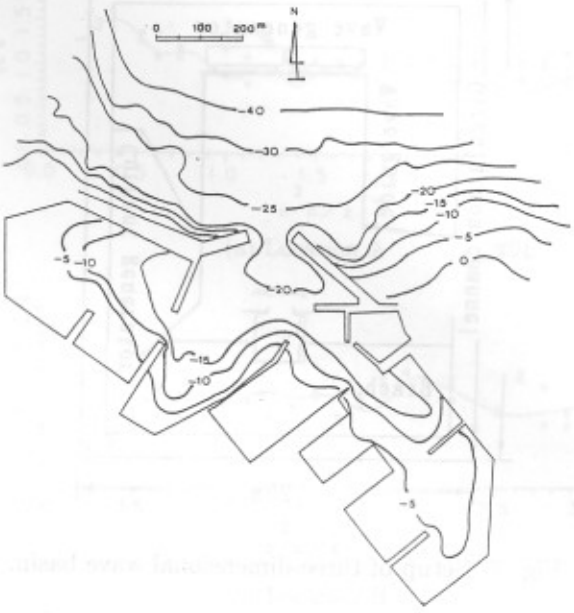

Fig. 5 Layout and topography of Patosu fishery harbour.

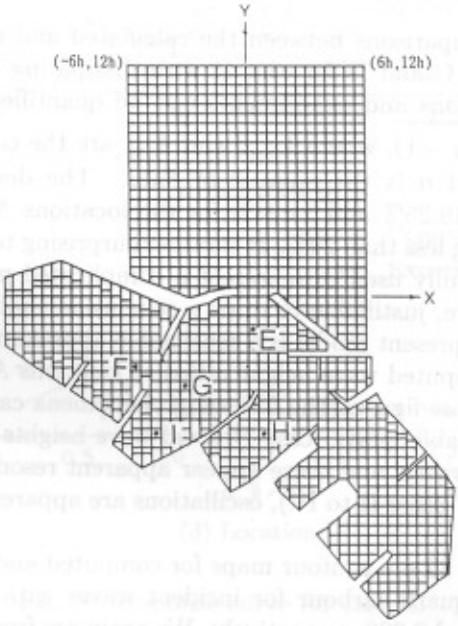

Fig. 6 Grid system and location of check points.

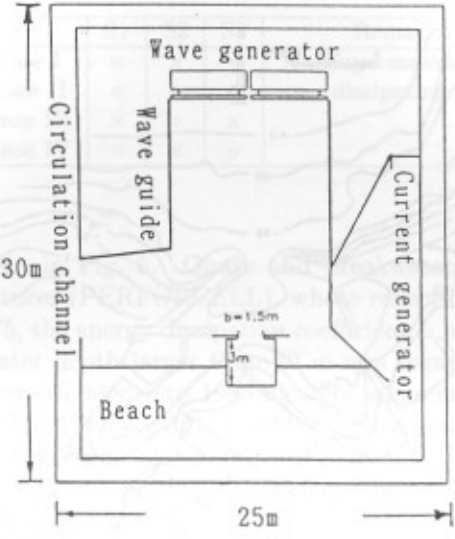

Fig. 7 Setup of three-dimensional wave basin.

VI. RESULTS OF COMPUTATIONS AND EXPERIMENTS

Figure 8 shows comparisons between the calculated and measured wave heights at the locations A, B, C and D for case II with dissipating quays. Agreement between numerical solutions and experiments can be quantified using deviation $v = \sqrt{\sum (\lambda_{num} - \lambda_{\exp})^2/(n-1)}$, where λ_{num} and $\lambda_{\exp}$ are the computed and measured wave height ratios and n is the number of data. The deviations obtained were v = 18.98%, 17.15%, 19.25% and 14.84% for the locations A, B, C and D, respectively, every value being less than 20%. It is rather surprising to see a fact that a single coefficient was successfully used to represent a complicated process of wave dissipation. It seems, therefore, justifiable to draw a conclusion that the energy dissipation coefficient used in the present model is a reasonable approximation.

Figure 9 shows computed wave height ratios at locations A, B, C and D for cases I through IV. From these figures, the following phenomena can be detected: (1) In a harbour with impermeable quays (case I), local wave heights largely fluctuates with frequency of incident waves, and there appear apparent resonances. (2) In harbours with dissipating quays (cases II to IV), oscillations are apparently reduced, especially in case II.

Figures 10 through 12 are contour maps for computed and measured wave height distributions in the square harbour for incident waves with angular frequencies of $\sigma^2 h/g$ =1.206, 0.537 and 0.302, respectively. We again see from these figures that the wave heights in the square basins with dissipating quays are apparently reduced,

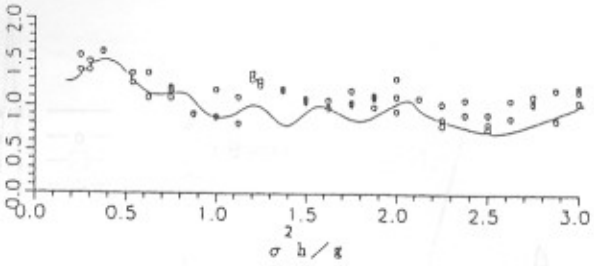

(a) Location A

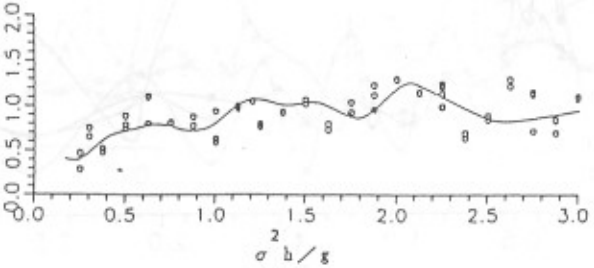

(b) Location B

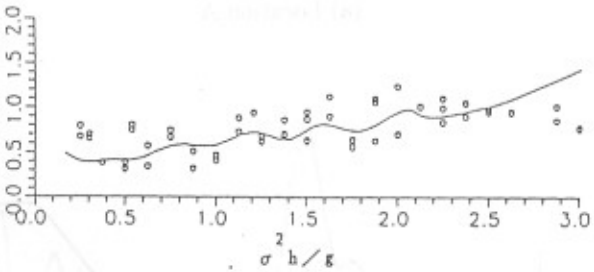

(c) Location C

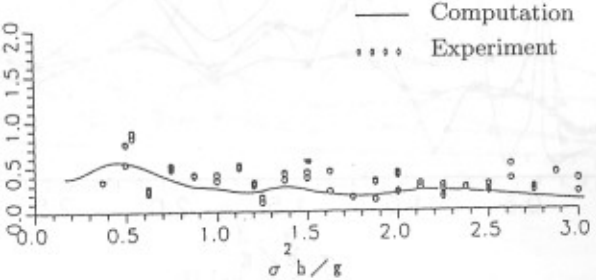

(d) Location D

Fig. 8 Response curve for case II.

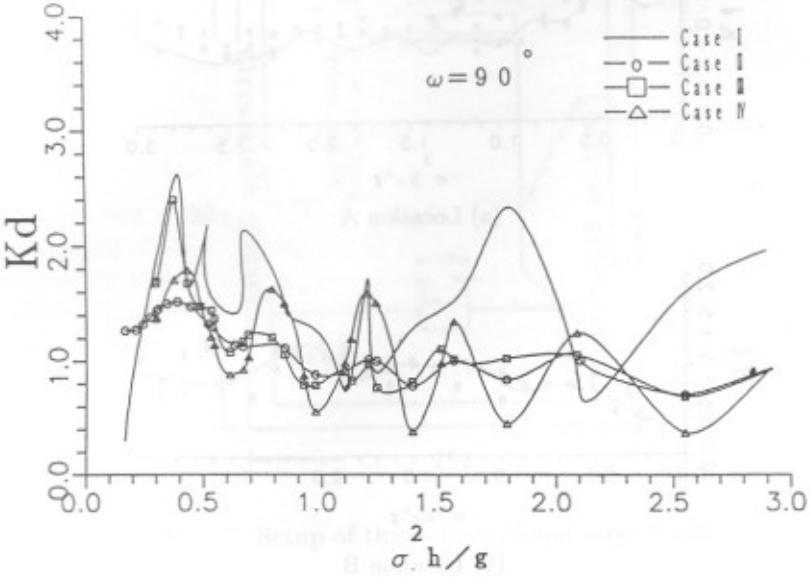

(a) Location A

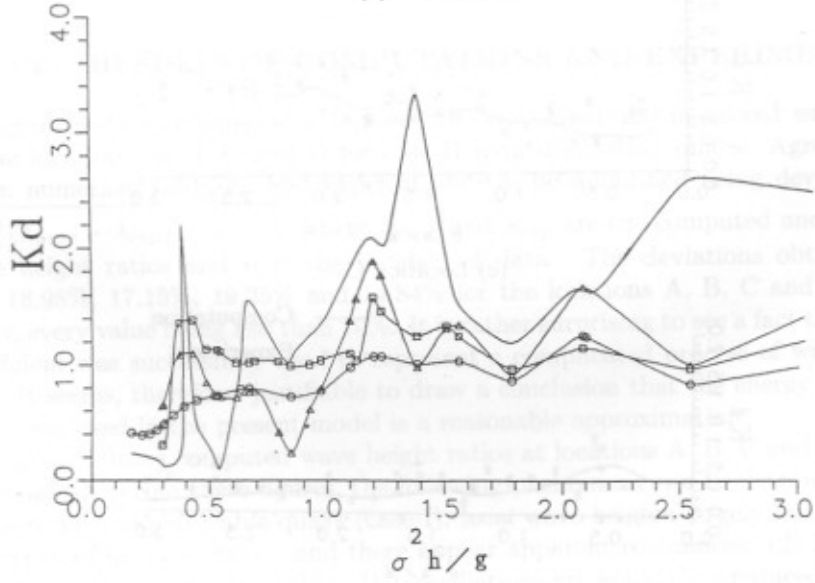

(b) Location B

Fig. 9 Wave heights at locations A to D. (continued)

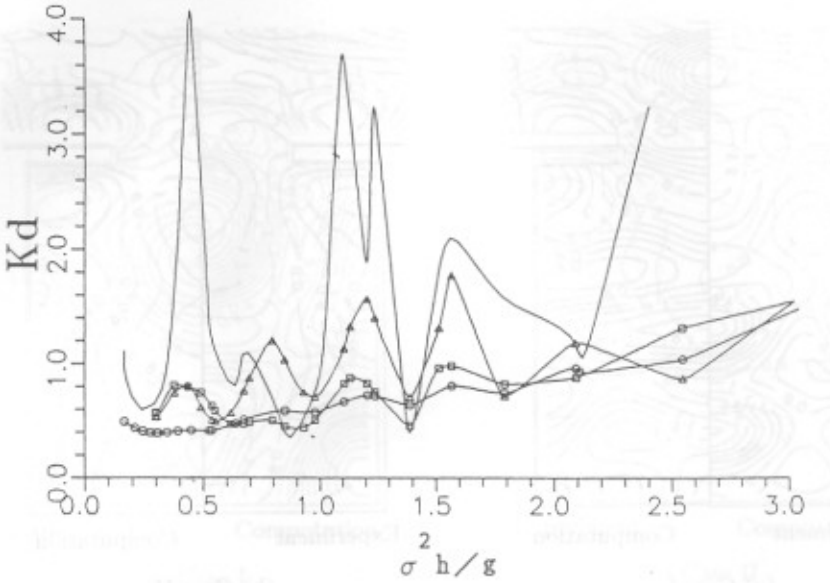

(c) Location C

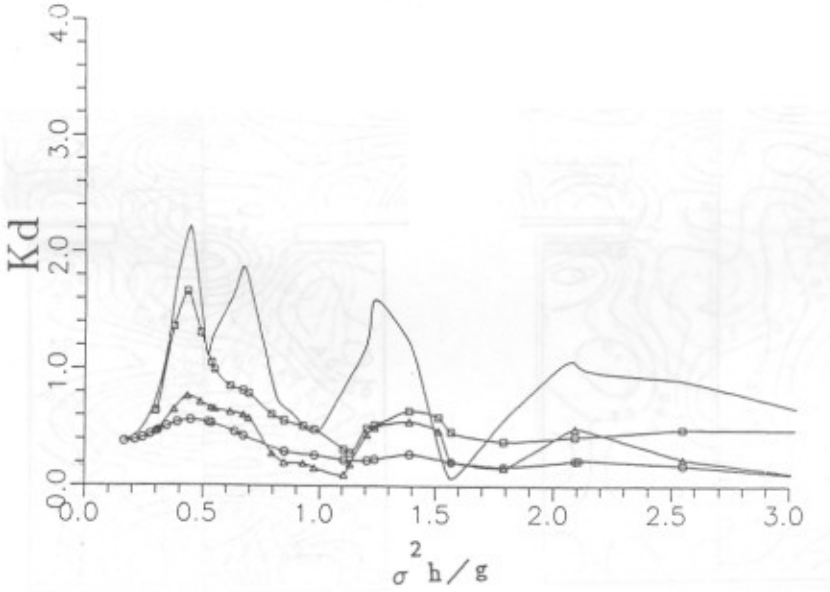

(d) Location D

Fig. 9 Wave heights at locations A to D.

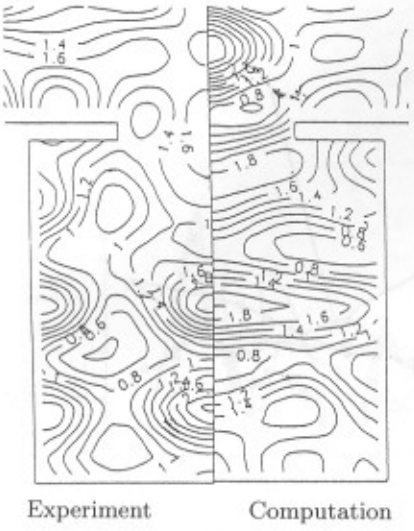

(a) Case I

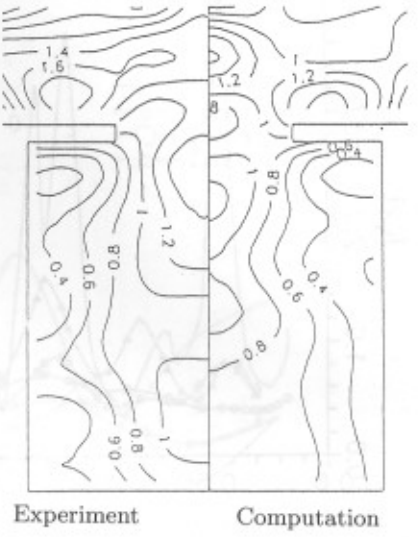

(b) Case II

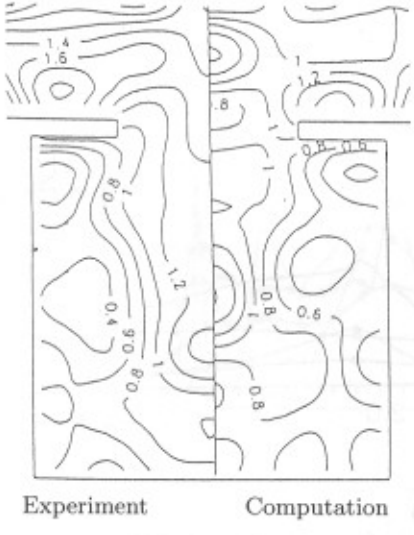

(c) Case III

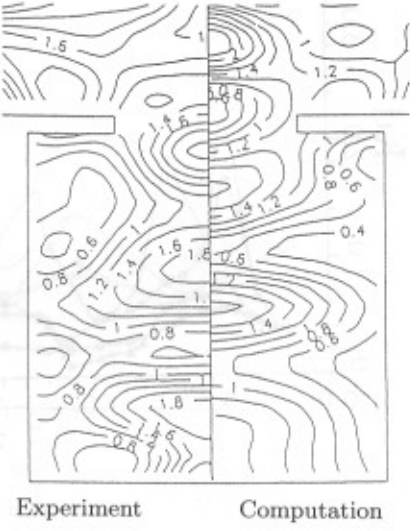

(d) Case IV

Fig. 10 Wave height distributions ($\sigma^2 h/g$=1.206, T=1.0 sec, h=30 cm, $\omega = 90°$).

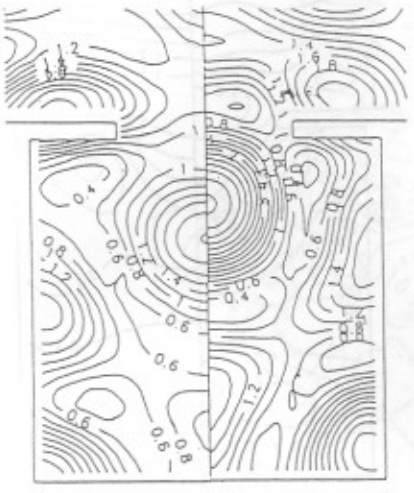

(a) Case I

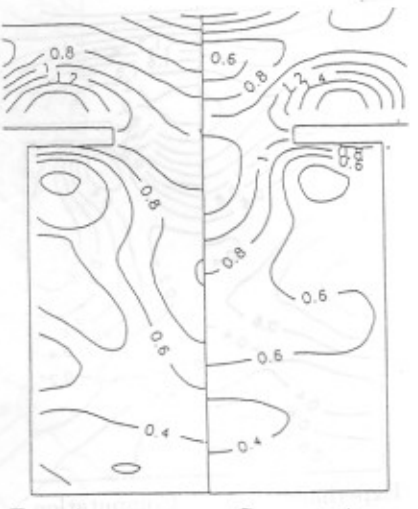

(b) Case II

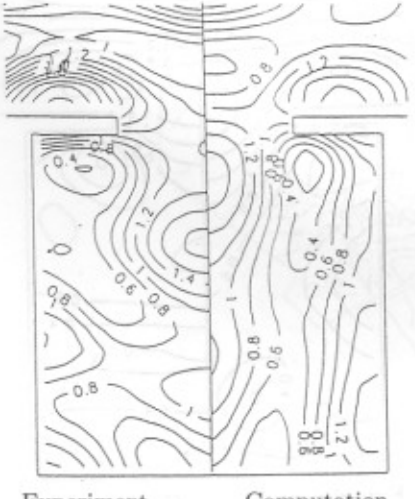

(c) Case III

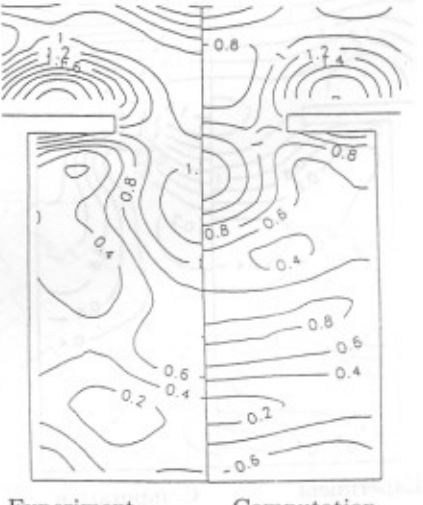

(d) Case IV

Fig. 11 Wave height distributions ($\sigma^2 h/g$=0.537, T=1.5 sec, h=30 cm, $\omega = 90°$).

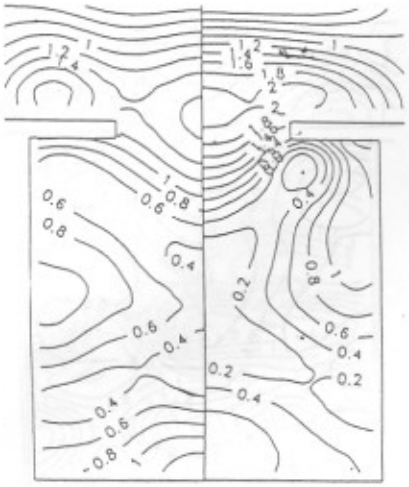

(a) Case I

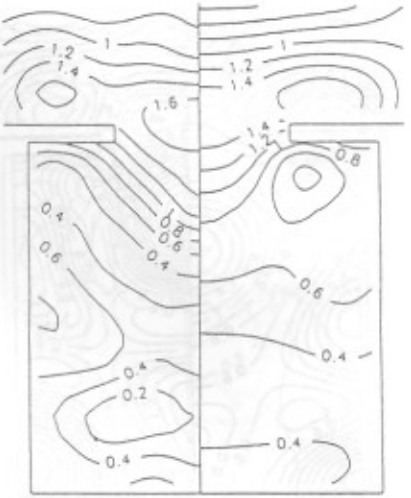

(b) Case II

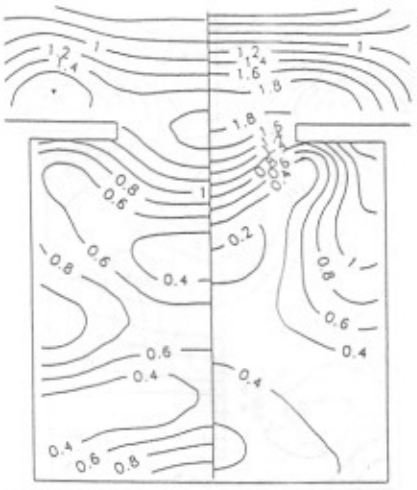

(c) Case III

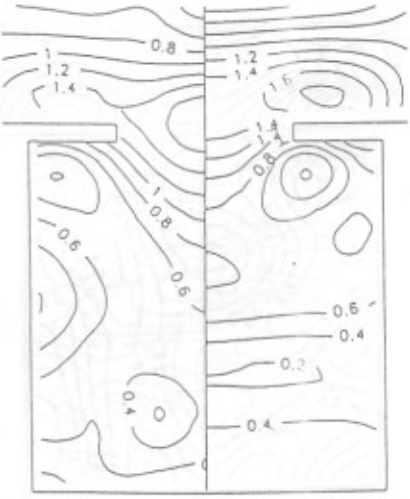

(d) Case IV

Fig. 12 Wave height distributions ($\sigma^2 h/g$=0.302, T=2.0 sec, h=30 cm, $\omega = 90°$).

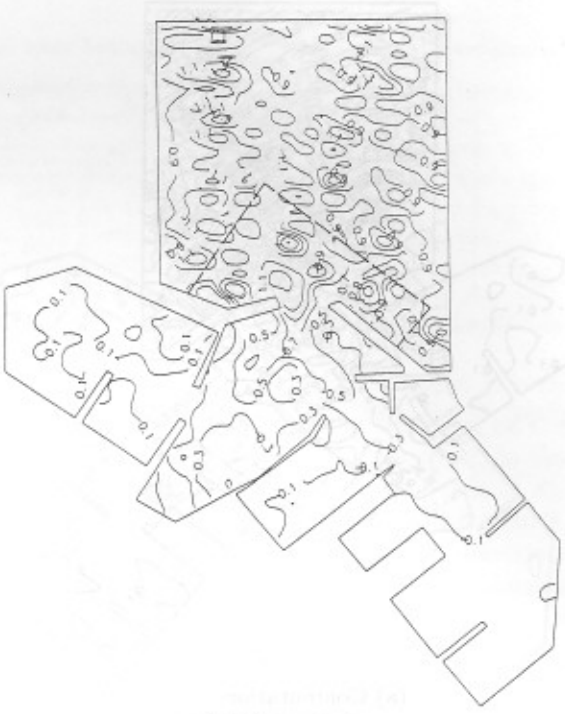

(a) Computation

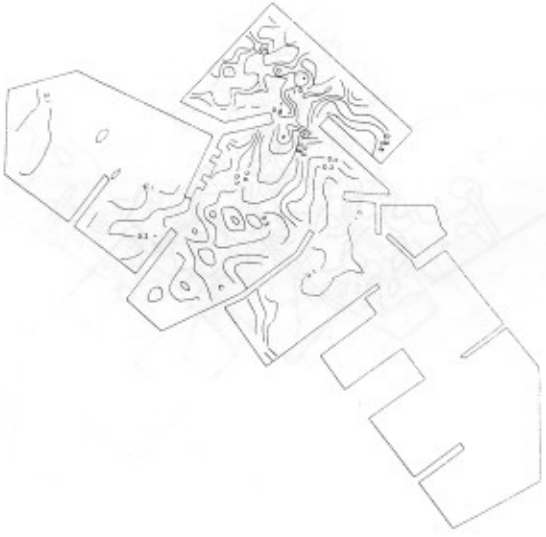

(b) Experiment

Fig. 13 Wave height distributions in Patosu fishery harbour (T=0.8 sec).

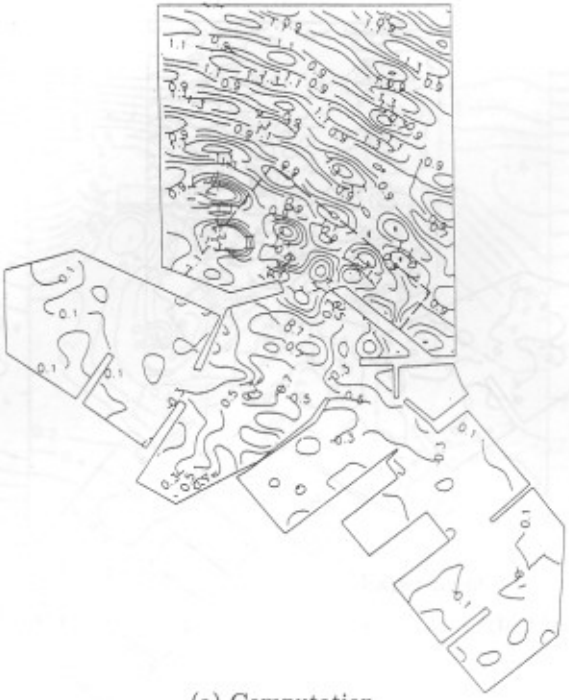

(a) Computation

(b) Experiment

Fig. 14 Wave height distributions in Patosu fishery harbour (T=1.0 sec).

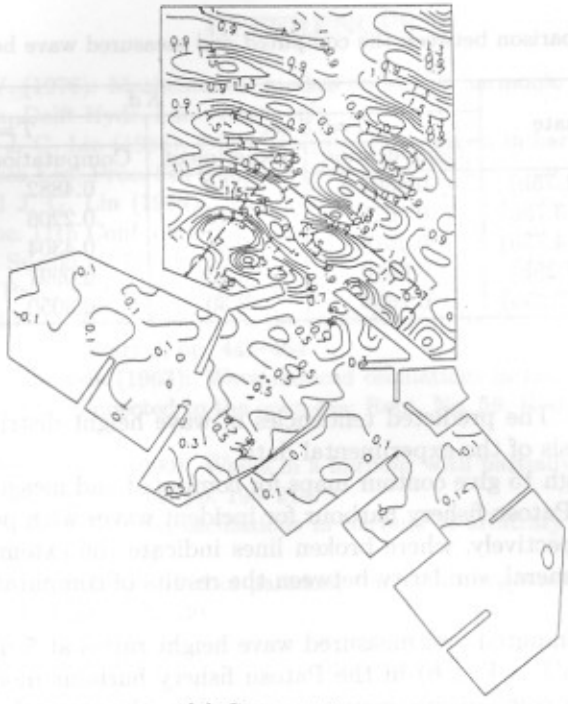

(a) Computation

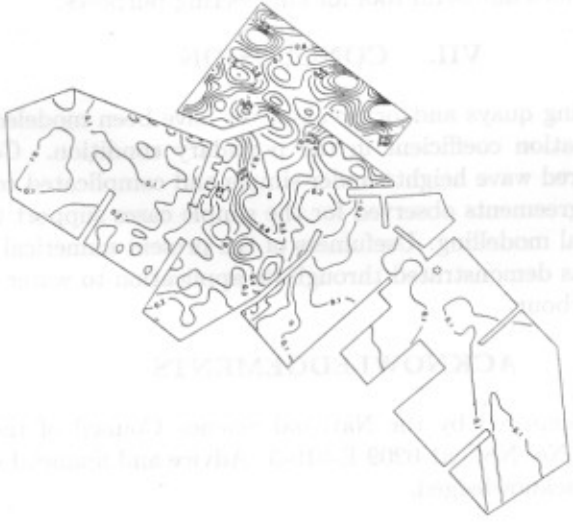

(b) Experiment

Fig. 15 Wave height distributions in Patosu fishery harbour (T=1.2 sec).

Table 2 Comparison between the computed and measured wave height ratios.

Location	Corrdinate	Kd			
		T=0.8 sec		T=1.0 sec	
		Computation	Experiment	Computation	Experiment
E	(0.25h, −1.75h)	0.4865	0.59	0.4882	0.63
F	(−5.75h, −3.75h)	0.1625	0.16	0.2206	0.10
G	(−3.25h, −4.75h)	0.4618	0.46	0.4304	0.29
H	(0.75h, −7.25h)	0.0810	0.13	0.0991	0.12
I	(−4.75h, −7.25h)	0.2658	0.30	0.3050	0.27

especially in case II. The predicted tendencies of wave height distributions are well confirmed on the basis of the experimental data.

Figures 13 through 15 give contour maps for computed and measured wave height distributions in the Patosu fishery harbour for incident waves with periods of T=0.8, 1.0 and 1.2 sec, respectively, where broken lines indicate the extent of wave height measurements. In general, similarity between the results of computations and experiments is reasonable.

Table 2 shows computed and measured wave height ratios at 5 measuring points (locations E through I in Fig. 6) in the Patosu fishery harbour model. A little deviation found in the comparisons may be ascribed to the phase lag depending on the material of dissipating structures, which is not considered in the computations. The results, however, are in satisfactory agreements, demonstrating that the present numerical model provides an useful tool for engineering purposes.

VII. CONCLUSION

Effects of dissipating quays and/or breakwaters have been modeled by introducing the energy dissipation coefficient in the boundary condition. Comparisons of calculated and measured wave heights under simple and complicated conditions were shown. Reasonable agreements observed for the simple cases support the use of this coefficient in numerical modelling. Usefulness of the present numerical model for engineering purposes was demonstrated through its application to water oscillations in the Patosu fishery harbour.

ACKNOWLEDGEMENTS

This study was sponsored by the National Science Council of the Republic of China under the grant No. NSC 81-0209-E-019-3. Advice and financial support of the council are gratefully acknowledged.

REFERENCES

Berkhoff, J. C. W. (1976): Mathematical models for simple harmonic water wave diffraction and refraction, Delft Hydr. Lab., Rept. 168.

Chou, C. R. and J. G. Lin (1986): BEM analysis of oscillation in harbor of arbitrary shape with uneven sea bed, Proc. 8th Conf. on Ocean Eng., R.O.C., pp. 111–130. (in Chinese)

Chou, C. R. and J. G. Lin (1989): Numerical analysis for harbour oscillation with wave absorber, Proc. 11th Conf. on Ocean Eng., R.O.C., pp. 365–381. (in Chinese)

Goda, Y. and Y. Suzuki (1976): Estimation of incident and reflected waves in random wave experiments, Proc. 15th Coastal Eng. Conf., ASCE, pp. 828–845.

Hwang, L. S. and E. O. Tuck (1970): On the oscillations of harbors of arbitrary shape, Jour. Fluid Mech., Vol. 42, Part 3, pp. 447–464.

Ippen, A. T. and Y. Goda (1963): Wave-induced oscillations in harbors: the solution for a rectangular harbor connected to the open-sea; Rept. No. 59, Hydrodynamics Lab., M. I. T.

Isaacson, M. and S. Q. Qu (1990): Waves in a harbour with partially reflecting boundaries, Coastal Engineering, Vol. 14, pp. 193–214.

Lee, J. J. (l971): Wave-induced oscillations in harbors of arbitrary geometry, Jour. Fluid Mech., Vol. 45, pp. 375–394.

Miles, J. and W. Munk (1961): Harbor paradox, Jour. Waterways and Harbors Div., ASCE, Vol. 87, No. WW3, pp. 111–130.

(Received Jan. 7, 1993; revised May 26, 1993)